INVESTIGATION OF THE THERMAL DECOMPOSITION OF TALC

Xiaowen Liu*, Xiaoxu Liu, and Yuehua Hu

School of Minerals Processing and Bioengineering, Central South University, Changsha 410083, China

Abstract—Different changes in the structural and thermal properties of various types of talc have been reported in the literature which have made comparison of analytical results difficult. The objective of the present study was to obtain some fundamental insights into the effects of the thermal behavior of talc and to carry out kinetic analyses of the decomposition of talc under high temperature. X-ray diffraction (XRD), Fourier-transform infrared spectroscopy (FTIR), and thermogravimetry-differential scanning calorimetry (TG-DSC) were used to study the thermal decomposition mechanism. The Coats-Redfern decomposition model was used to determine the decomposition mechanism of talc samples. The results showed that the decomposition of talc commenced at ~800ºC, peaking at ~895ºC, with the formation of enstatite and amorphous silica. An isothermal treatment at 1000ºC caused the complete dehydroxylation of talc. The XRD and FTIR results indicated that the enstatite and amorphous silica phases were transformed into clinoenstatite and paracrystalline opal phases, respectively, after the decomposition stage at 1200ºC. Good linearity in the Coats-Redfern model was observed from room temperature to 1300ºC and the activation energy was calculated to be 69 kcal/mol.

Key Words—Activation Energy, Coats-Redfern, Thermal Decomposition, Talc.

INTRODUCTION

Talc, $Mg_3Si_4O_{10}(OH)_2$, is used widely in the form of a fine powder in several industrial applications such as ceramics (Ptáček *et al*., 2014), pharmaceutical (Lee *et al*., 2010; Akhtar *et al*., 2012), cosmetics (Agarwal *et al*., 2011), and papermaking (Yu *et al*., 2013), and as a filler in talc-polymer composites to enhance nucleation and improve the mechanical properties (Dellisanti *et al*., 2011). It is the 2:1 trioctahedral ene-member phyllosilicate (Drits *et al*., 2012; Schumann *et al*., 2013). Recently, possible changes in the properties of talc during high-temperature calcination have received a great deal of attention because the changes in the physico-chemical, structural, and thermal properties of talc can be exploited in new industrial applications, such as foamed glass (Okada *et al*., 2009), oil lubricants (Prasad *et al*., 2010), and electronic substrates for integrated circuits (Gökçe *et al*., 2011). The influence of mechanical grinding (Christidis *et al*., 2004; Terada and Yonemochi, 2004; Dellisanti *et al*., 2009, 2011; Zulumyan *et al*., 2012) and sonication treatments (Jamil and Palaniandy, 2010; Şener and Özyılmaz, 2010; Jamil and Palaniandy, 2011) on the talc structure have been analyzed extensively. The main effects described in those studies are the progressive structural disorder and subsequent amorphization of the material leading to changes in its physical and thermal properties (Palaniandy and Azizli, 2009; Mahadi and Palaniandy, 2010), and only demonstrate the deformation of talc under relatively low-temperature conditions.

Previous studies have described the decomposition of talc under thermal treatment. The formation of beta magnesium metasilicate was reported at ~600ºC by Avgustinik and Vigdergauz (1948) who also suggested that at 1200ºC silica was dissolved and recrystallized as enstatite. The dehydroxylation temperature was reported by Kedesdy (1943) to be 800ºC, however, with the formation of enstatite only, and protoenstatite formed at 1400ºC. The formation of enstatite, amorphous silica, and water vapor when talc was decomposed at 800−840ºC was noted by Ewell *et al*. (1935). The enstatite changed gradually to protoenstatite at ~1200ºC, and the amorphous silica was converted to cristobalite at ~1300ºC. The dehydroxylation of talc was reported by Ptáček *et al*. (2014) to occur at ~905ºC; enstatite, amorphous silica, and water were formed during this process and cristobalite in particular was stated to originate from the silica phase at 1150ºC. Talc was reported (Dellisanti and Valdrè, 2010) to dehydroxylate in a single step to form $MgSiO_3$ and cristobalite from 1473 to 1600ºC. Comparison of results, however, is difficult because of the various types of dehydroxylation reaction proposed in all these reports.

The objectives of the present study were to obtain insights into the effects of the thermal behavior of talc, to carry out kinetic analysis of its decomposition at high temperatures, and to test the applicability of the Coats-Redfern decomposition model to talc.

EXPERIMENTAL

Materials and methods

Talc was obtained from Guangxi Longguang Talc Development Co. Ltd., China, with chemical compositions listed in Table 1. The talc content was >98 wt.%.

* E-mail address of corresponding author:
onlylonely101@126.com

Table 1. Chemical compositions (mass %) of different samples by XRF.

Samples	SiO_2	MgO	Al_2O_3	Fe_2O_3	CaO
'Original' talc	67.68	31.04	0.77	0.50	0.01
200ºC	65.20	33.33	0.47	0.50	0.02
700ºC	65.64	33.36	0.49	0.50	0.02
800ºC	65.66	33.33	0.48	0.52	0.02
900ºC	65.73	33.25	0.50	0.50	0.02
1000ºC	65.70	33.34	0.44	0.50	0.02

After drying at 60ºC, talc was ground into a powder *via* a planetary ball mill to pass through a 0.074 mm sieve and this was labeled as the 'original' talc sample. Analysis of the talc sample by scanning electron microscopy (SEM) (Figure 1) revealed the morphology and size of the aggregated particles to be within the 5−30 μm range.

4-g samples of 'original' talc were heated in a programmed temperature-controlled muffle furnace at scheduled temperatures (200−1300ºC) for 2.5 h. The heating rate, β, was 10ºC/min. The products were ground into powders using an agate mortar and were given names denoted by the heating temperature (ºC).

Phosphoric-acid digestion was applied to the 1200ºC sample. Orthophosphoric acid (H_3PO_4, 85% mass content; density of 1.71 g cm^{-3}) was supplied by JT Baker Chemical Company (Phillipsburg, New Jersey, USA) − 2 g of the 1200ºC sample was mixed with 100 mL of H_3PO_4 and the mixture heated rapidly to 240ºC and maintained at that temperature for 12 min. After the viscous solution was cooled to 60ºC, it was then diluted with distilled water to 800 mL and filtered. The residue was washed with distilled water to remove the excess PO_4^{3-} ions and dried at room temperature. This phosphoric-acid digestion sample was labeled 'K0'.

Characterization techniques

X-ray diffraction patterns were obtained using a DX-2700 instrument (Dandong Haoyuan Instrument Co. Ltd., China) with an acceleration voltage of 40 kV and an emission current of 40 mA at a scanning rate of 9º/min from 3 to 80º2θ. Fourier-transform infrared (FTIR) spectra were recorded using a Nicolet 5700 spectrophotometer (Thermo Nicolet, USA). The specimens used for FTIR measurement were prepared by mixing 0.9 mg of sample powder with 80 mg of KBr and pressing the mixture into a pellet. The morphology of the samples was examined by SEM (Sirion 200, FEI, USA). Thermogravimetry-differential scanning calorimetry (TG-DSC) was performed at heating rates, β, of 12ºC/min under N_2 atmosphere (20 cm^3/min) with masses of 10 mg using a Netzch STA449C thermal analyzer (Netzsch, Germany). α-Al_2O_3 was used as an inert material. The chemical compositions of the talc were measured by X-ray fluorescence (XRF, Axios max, PANalytical, Netherlands).

RESULTS AND DISCUSSION

The XRD pattern of the 'original' talc sample (Figure 2a) showed that all of the diffraction peaks observed were indexed to the characteristics of talc (JCPDS 19-0770). Over the range 200−700ºC, the locations of most talc peaks changed little. Calcination produced a decrease in the intensity and led to broadening of the diffraction lines; changes in the (001) planes at 9.3º in particular were attributed to a decrease in crystallinity (Yang *et al.*, 2006). The change in crystallinity was used to quantify the progressive structural damage (Aglietti and Potto Lopez, 1992). This index included the background and peak intensities, defining crystallinity as $C = B_0I/(I_0B) \times 100\%$, where C was the crystallinity, B_0 was the background intensity for 'original' material, I was the peak intensity for thermally treated material, I_0 was the peak intensity for 'original' material, and B was the background intensity for thermally treated material. The corresponding (001) plane crystallinities of the original, 200ºC, 300ºC, 400ºC, 500ºC, 600ºC, and 700ºC talc samples were 100, 63.4, 59.3, 52.7, 47.6, 36.8, and 32.2%, respectively. Moreover, decreasing d values were noted at increasing temperatures from 200 to 700ºC (Table 2), *e.g.*
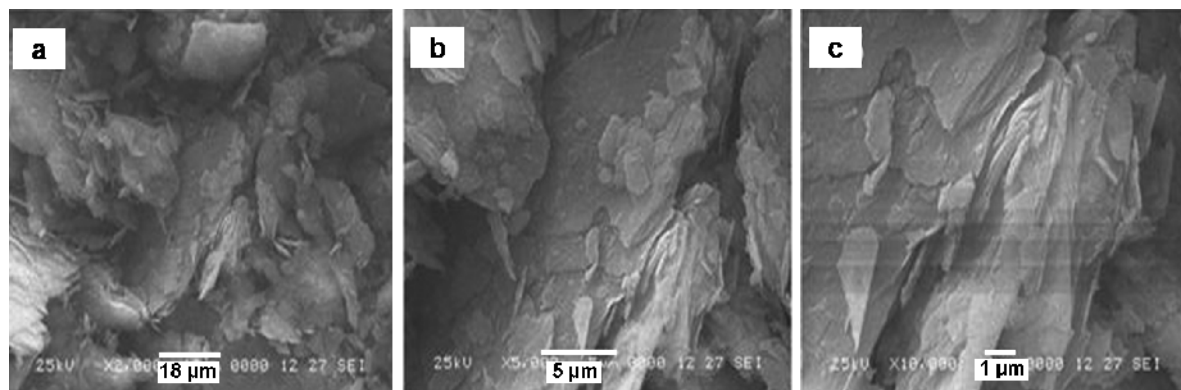

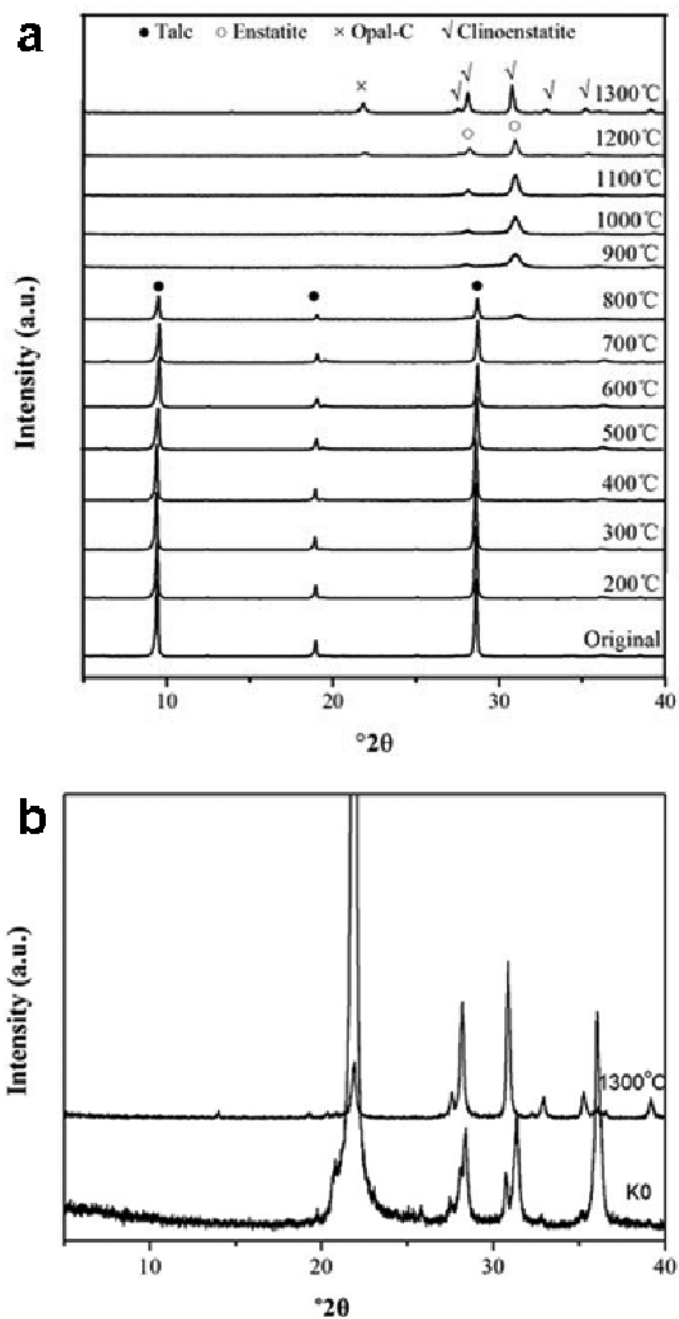Figure 1. SEM images of the 'original' talc sample.

Figure 2. XRD patterns of various samples (a) and of samples at 1300ºC and the K0 sample (b).

d_{001} changed from 0.94 to 0.92 nm and d_{002} from 0.47 to 0.46 nm. Dehydration of talc occurred over the temperature range from 200 to 700ºC.

One new peak was observed at 30.7º2θ in the 800ºC sample, due to enstatite, according to the JCPDS 19-0768 powder diffraction file. The appearance of enstatite indicated that dehydroxylation of talc had begun at 800ºC. The intensity of this new peak increased during and after the dehydroxylation process, especially the (610) plane of enstatite (the intensity of the (610)

Table 2. The basal d values of peaks for different samples.

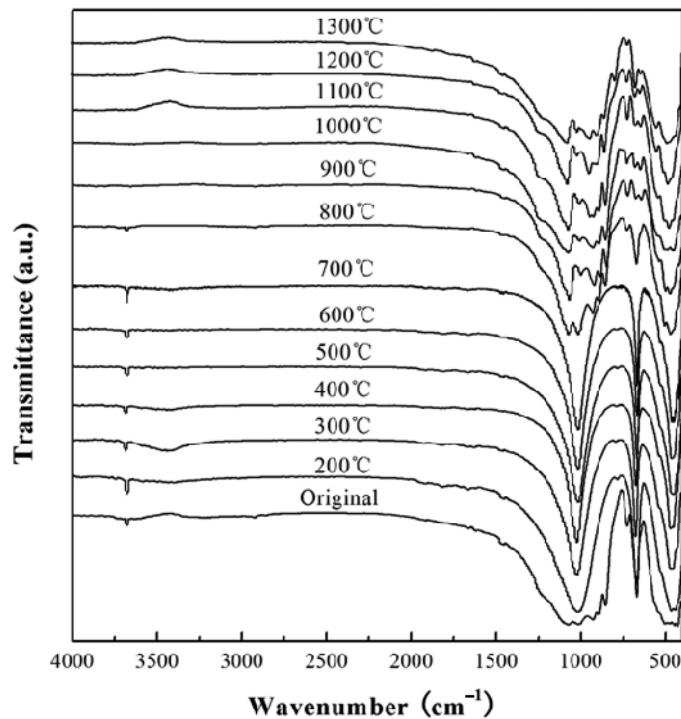| Samples	d_{001} (nm)	d_{002} (nm)	d_{208} (nm)
'Original' talc	0.94	0.47	0.19
200ºC	0.94	0.47	0.19
300ºC	0.94	0.47	0.19
400ºC	0.94	0.47	0.19
500ºC	0.93	0.47	0.19
600ºC	0.92	0.47	0.19
700ºC	0.92	0.47	0.19

Figure 3. FTIR spectra of various samples.

plane increased from 44 to 530 counts over the temperature range 800 to 1200ºC), which was attributed to the increasing crystallization and crystallite size of enstatite which enlarged from 15.0 to 43.2 nm over that temperature range. As the calcination temperature increased, another new, weak peak occurred at 21.9º2θ in the 1200ºC sample; according to the JCPDS 39-1425 powder diffraction file, this peak is characteristic of paracrystalline opal (Elzea *et al.*, 1994; Sarıkaya *et al.*, 2000; Önal and Sarıkaya, 2007). The corresponding 'K0' sample produced an XRD pattern with the characteristic paracrystalline opal (opal-C) peak, d_{101} = 0.41 nm. After heating at 1050ºC for 24 h, the full width at half-maximum (FWHM) of the 101 reflection was unchanged, shifted from 21.9 to 21.8º2θ, and intensified by a factor of at least two (Figure 2b), clearly indicating

that opal-C had been formed (Önal *et al.*, 2007). The enstatite phase was transformed to clinoenstatite in the 1300ºC sample. The peak at 30.7º2θ shifted to 31.7º2θ and a new peak at 27.5º2θ appeared, characteristic of clinoenstatite according to JCPDS 35-0610.

The FTIR spectra of talc samples at different calcination temperatures (Figure 3) revealed that the increasing temperature had a great effect on the structure of talc (detailed assignments of each band shown in Table 3). The 'original' talc sample possessed obvious signals as reported by Mollah *et al.* (1999) and Castillo *et al.* (2013), such as 428 (Si−O), 465 (Si−O−Si), and 671 cm^{-1} (Si−O−Mg). As the temperature increased from 200 to 700ºC, the Si−O−Si stretching vibration shifted from 1013 to 1019 cm^{-1} with the progressive intensity caused by the dehydration of talc (Jamil and

Table 3. The assignments of bands for different samples.

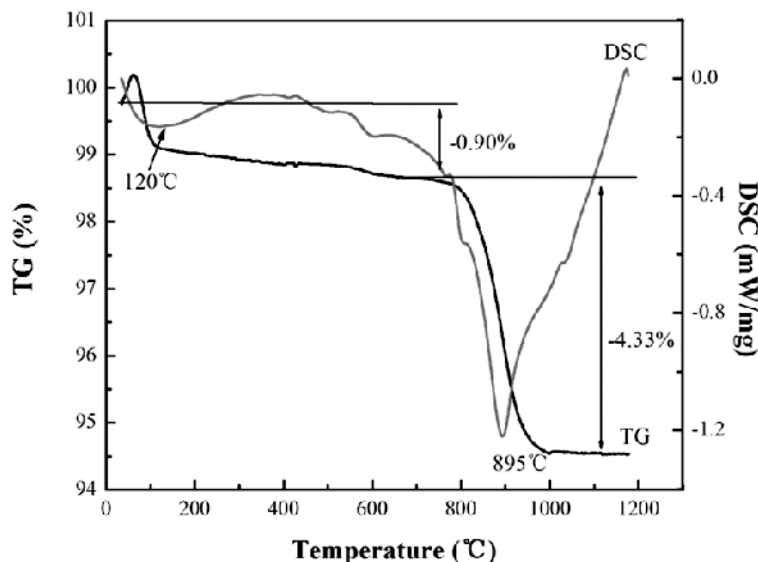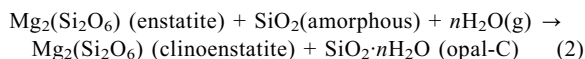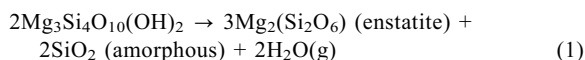| Vibrational frequency (cm^{-1})	Assignment
3678	Stretching vibration of Mg−OH
~3429−3474	OH-stretching vibration of absorbed water
~1635−1654	OH-bending vibration of absorbed water
~1017−1094	Stretching vibration of Si−O−Si
671	Stretching vibration of Si−O−Mg
~465−472	Bending vibration of Si−O−Si
428	Stretching vibration of Si−O

Figure 4. TG-DSC curves of the 'original' talc sample.

Palaniandy, 2011). Compared to the 700ºC sample, the IR spectrum of the 800ºC sample displayed two weaker bands at 672 and 1016 cm^{-1} and they originated from the stretching vibrations of Si−O−Mg (Jamil and Palaniandy, 2011) and Si−O−Si, respectively (Dellisanti *et al*., 2009). The decreasing intensity of these two bands was attributed to the dehydroxylation of talc at 800ºC. The new peaks at 1072, 929, 895, 855, 727, and 505 cm^{-1} were assigned to enstatite in accordance with previous studies (Goel *et al*., 2009) and indicated that enstatite had been generated at 800ºC as shown by the XRD results. The intensity of the asymmetrical stretching vibration of Si−O−Si at 1072 cm^{-1} increased as the temperature increased from 800 to 1300ºC and the position shifted from 1072 to 1076 cm^{-1}, possibly related to changes in the molecular structure of enstatite after heating at temperatures in excess of 800ºC (Goel *et al*., 2009). Moreover, an indication of the formation of amorphous silica was observed in the 800ºC sample by the new absorption bands at ~895 and ~929 cm^{-1}, which were consistent with a transparent silica window (~860−960 cm^{-1}) (Inaki *et al*., 2002). The intensity of bands at 895 and 928 cm^{-1} increased from 800 to 1200ºC, and then decreased at 1300ºC. The Mg−OH stretching vibration band at 3678 cm^{-1} weakened gradually from 200 to 1000ºC and disappeared after 1000ºC, indicating that dehydroxylation of talc is completed after heating to 1000ºC. The transformation of amorphous silica to opal-C occurred from 1200 to 1300ºC as the band at 794 cm^{-1}, attributed to opal-C, appeared at 1300ºC (Mollah *et al*., 1999).

The TG-DSC curves of 'original' talc samples (Figure 4) showed that a small weight loss of ~0.9% at 120ºC was due to the loss of absorbed water (Dellisanti and Valdrè, 2010; Wang and Karato, 2013). In the TG curves of talc, a significant weight loss occurred over the temperature range from 800 to 1000ºC with a broad endothermic DSC signal peak at 894ºC related to the dehydroxylation of talc (equation 1), consistent with previous results of dehydroxylation of talc from 800 to 1000ºC (Smykatz-Kloss, 1974; Ward, 1975; Paterson and Swaffield, 1987; Okada *et al*., 2009). Enstatite, amorphous silica, and water were formed during this process and the total weight loss was ~4.3%. The diffraction lines of enstatite appeared on the XRD plot in this temperature range. Opal-C (SiO$_2$·nH$_2$O) originated from the silica phase at 1200ºC. The following reaction may take place at high temperature:

$$2Mg_3Si_4O_{10}(OH)_2 \rightarrow 3Mg_2(Si_2O_6) \text{ (enstatite)} + 2SiO_2 \text{ (amorphous)} + 2H_2O(g) \qquad (1)$$

$$Mg_2(Si_2O_6) \text{ (enstatite)} + SiO_2\text{(amorphous)} + nH_2O(g) \rightarrow Mg_2(Si_2O_6) \text{ (clinoenstatite)} + SiO_2·nH_2O \text{ (opal-C)} \qquad (2)$$

The reaction temperatures of equations 1 and 2 were ~800 and 1200ºC, respectively, in accordance with the results obtained by Wesolowski (1984), who reported that the decomposition of talc was accompanied by the formation of enstatite and amorphous silica. The inversion of enstatite to clinoenstatite took place gradually, both phases being observed in the material heated at 1200ºC. The presence of clinoenstatite alone had been detected at temperatures as high as 1300 to 1435ºC.

All kinetic studies envisage one of two methods: differential or integral. All the methods are based on the kinetic equation (Tang *et al*., 2003):

$$d\alpha/dt = k(1-\alpha)^n = A\exp(-E/RT)(1-\alpha)^n \qquad (3)$$

Table 4. Relation between the transformation rate (α) of talc samples and the reaction temperature (T).

β (K·min^{-1})	T (K)										
	$\alpha = 0\%$	$\alpha = 10\%$	$\alpha = 20\%$	$\alpha = 30\%$	$\alpha = 40\%$	$\alpha = 50\%$	$\alpha = 60\%$	$\alpha = 70\%$	$\alpha = 80\%$	$\alpha = 90\%$	$\alpha = 100\%$
12	1065	1102	1122	1138	1150	1160	1171	1181	1195	1214	1408

where $d\alpha/dt$ was the decomposition rate; n, the degree of the decomposition reaction; A, the frequency factor; E, the activation energy of the decomposition; T, the absolute temperature; R, the gas constant; α, the transformation rate; and k, the decomposition rate constant.

The integral method approach to the kinetic study was more convenient, reliable, and accurate than the differential method (Tang *et al.*, 2003). In the present investigation, therefore, the Coats-Redfern method, an integral approach, was followed to investigate the decomposition kinetics of talc. The Coats-Redfern method is based on the equation (Qin *et al.*, 2005):

$$\ln[g(\alpha)/T^2] = \ln[AR(1-2RT/E)/\beta E] - E/RT \qquad (4)$$

where $g(\alpha) = -\ln(1-\alpha)$, for $n = 1$; $g(\alpha) = [1-(1-\alpha)^{1-n}]/(1-n)$, for $n \neq 1$. Different n values were substituted into equation 4 and $\ln[g(\alpha)/T^2]$ was plotted *vs.* $1/T$. The n value that gave the best fit (maximum correlation coefficient) was taken as the reaction order (Qin *et al.*, 2005). The Coats-Redfern method has been used successfully to analyze the decomposition of ammonium pentaborate (Şahin *et al.*, 2001), poly(ethylene terephthalate)/clay nanocomposites (Xu *et al.*, 2010), and BaCO$_3$ (Maitra and Bandyopadhyay, 2008). The decomposition of talc was a typical example of a solid-state reaction. The reaction followed first-order kinetics. In order to confirm the mechanism function, the data for

the relation between the transformation rate of the talc samples (α) and reaction temperature (T) were used in the Coats-Redfern-method calculations. The variation in α as a function of temperature is shown in Table 4.

By making some mathematical approximations to the above equation and taking its integral, the following Coats-Redfern equation for $n = 1$ was obtained.

$$\ln[-\ln(1-\alpha)/T^2] = \ln[AR(1-2RT/E)/\beta E] - E/RT \qquad (5)$$

The slope of the plot of $\ln[-\ln(1-\alpha)/T^2]$ *vs.* $1/T$ yields $-E/R$, meaning that if the plot is linear the activation energy can be calculated. The graph of $\ln[-\ln(1-\alpha)/T^2]$ *vs.* $1/T$ (Figure 5) indicates good linearity, suggesting it as a suitable model for this process. The value of E was calculated to be 69 kcal/mol.

CONCLUSIONS

TG-DSC was used to investigate the thermal decomposition process of talc at constant heating rate under an N$_2$ atmosphere; data from XRD and FTIR analyses were used to confirm this determination. Talc transformed to enstatite after heating to 800ºC and the dehydroxylation peak temperature was ~895ºC. After 1000ºC, talc dehydroxylated completely. The XRD and FTIR results indicated that the enstatite and amorphous silica phases were transformed to clinoenstatite and opal-C phases, respectively, after dehydroxylation at 1200ºC. The
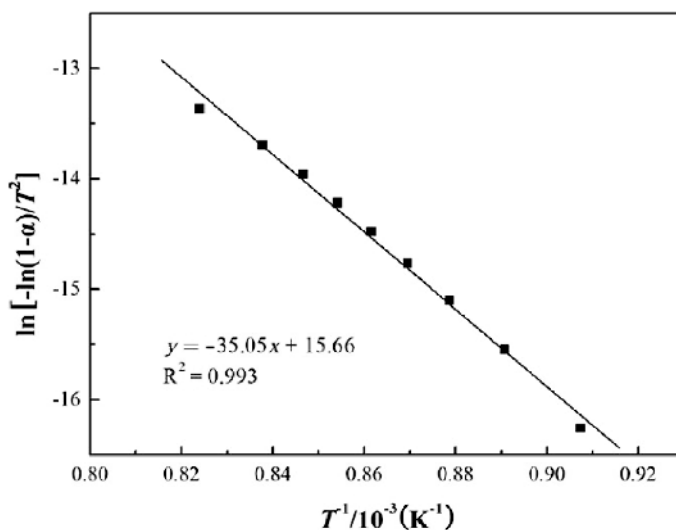

Figure 5. Calculation of the activation energy of talc samples using the Coats-Redfern integral method.

reaction kinetics model of talc decomposition in a solid-state reaction was researched based on a chosen mechanism function − the Coats-Redfern method. The mechanism of talc decomposition was confirmed and the activation energy was calculated to be 69 kcal/mol.

ACKNOWLEDGMENTS

REFERENCES

Agarwal, R., Paul, A.S., Aggarwal, A.N., Gupta, D., and Jindal, S.K. (2011) A randomized controlled trial of the efficacy of cosmetic talc compared with iodopovidone for chemical pleurodesis. *Respirology*, **16**, 1064−1069.

Aglietti, E.F. and Potto Lopez, J.M. (1992) Physicochemical and thermal properties of mechanochemically activated talc. *Materials Research Bulletin*, **27**, 1205−1216.

Akhtar, M.J., Ahamed, M., Khan, M.A.M., Alrokayan, S.A., Ahmad, I., and Kumar, S. (2012) Cytotoxicity and apoptosis induction by nanoscale talc particles from two different geographical regions in human lung epithelial cells. *Environmental Toxicology*, doi:10.1002/tox.21766.

Avgustinik, A.I. and Vigdergauz, V.S. (1948) Properties of talc during heating. *Ogneupory*, **13**, 218−227

Castillo, L., López, O., López, C., Zaritzky, N., García, M.A., Barbosa, S., and Villar, M. (2013) Thermoplastic starch films reinforced with talc nanoparticles. *Carbohydrate Polymers*, **95**, 664−674.

Christidis, G.E., Makri, P., and Perdikatsis, V. (2004) Influence of grinding on the structure and colour properties of talc, bentonite and calcite white fillers. *Clay Minerals*, **39**, 163−175.

Dellisanti, F. and Valdrè, G. (2010) On the high-temperature structural behaviour of talc ($Mg_3Si_4O_{10}(OH)_2$) to 1600ºC: effect of mechanical deformation and strain. *Philosophical Magazine*, **90**, 2443−2457.

Dellisanti, F., Valdrè, G., and Mondonico, M. (2009) Changes of the main physical and technological properties of talc due to mechanical strain. *Applied Clay Science*, **42**, 398−404.

Dellisanti, F., Minguzzi, V., and Valdrè, G. (2011) Mechanical and thermal properties of a nanopowder talc compound produced by controlled ball milling. *Journal of Nanoparticle Research*, **13**, 5919−5926.

Dritis, V.A., Guggenheim, S., Zviagina, B.B., and Kogure, T. (2012) Structures of the 2:1 layers of pyrophyllite and talc. *Clays and Clay Minerals*, **60**, 574−587.

Elzea, J.M., Odom, I.E., and Miles, W.J. (1994) Distinguishing well ordered opal-CT and opal-C from high temperature cristobalite by X-ray diffraction. *Analytica Chimica Acta*, **286**, 107−116.

Ewell, R.H., Bunting, E.N., and Geller, R.F. (1935) Thermal decomposition of talc. *Journal of Research of the National Bureau of Standards*, **15**, 551−556.

Goel, A., Tulyaganov, D.U., Shaaban, E.R., Knee, C.S., Eriksson, S., and Ferreira, J.M.F. (2009) Structure and crystallization behaviour of some $MgSiO_3$-based glasses. *Ceramics International*, **35**, 1529−1538.

Gökçe, H., Ağaoğulları, D., Öveçoğlu, M.L., Dumana, İ., and Boyraz, T. (2011) Characterization of microstructural and thermal properties of steatite/cordierite ceramics prepared by using natural raw materials. *Journal of the European Ceramic Society*, **31**, 2741−2747.

Inaki, Y., Yoshida, H., Yoshida, T., and Hattori, T. (2002)

Active sites on mesoporous and amorphous silica materials and their photocatalytic activity: an investigation by FTIR, ESR, VUV-UV and photoluminescence spectroscopies. *Journal of Physical Chemistry B*, **106**, 9098−9106.

Jamil, N.H. and Palaniandy, S. (2010) Acid medium sonication: A method for the preparation of low density talc nanosheets. *Powder Technology*, **200**, 87−90.

Jamil, N.H. and Palaniandy, S. (2011) Comparative study of water-based and acid-based sonications on structural changes of talc. *Applied Clay Science*, **51**, 399−406.

Kedesdy, H. (1943) Electron-microscope investigation of firing of talc and soapstone. *Berichte der Deutschen Keramischen Gesellschaft*, **24**, 201−232.

Lee, P., Sun, L., Lim, C.K., Aw, S.E., and Colt, H.G. (2010) Selective apoptosis of lung cancer cells with talc. *European Respiratory Journal*, **35**, 450−452.

Mahadi, M.I. and Palaniandy, S. (2010) Mechanochemical effect of dolomitic talc during fine grinding process in mortar grinder. *International Journal of Mineral Processing*, **94**, 172−179.

Maitra, S. and Bandyopadhyay, N. (2008) Application of non-Arrhenius method for analyzing the decomposition kinetics of $SrCO_3$ and $BaCO_3$. *Journal of the American Ceramic Society*, **91**, 337−341.

Mollah, M.Y.A., Promreuk, S., Schennach, R., Cocke, D.L., and Güler, R. (1999) Cristobalite formation from thermal treatment of Texas lignite fly ash. *Fuel*, **78**, 1277−1282.

Okada, K., Ikawa, F., Isobe, T., Kameshima, Y., and Nakajima, A. (2009) Low temperature preparation and machinability of porous ceramics from talc and foamed glass particles. *Journal of the European Ceramic Society*, **29**, 1047−1052.

Önal, M. and Sarıkaya, Y. (2007) The effect of heat treatment on the paracrystallinity of an opal-CT found in a bentonite. *Journal of Non-Crystalline Solids*, **353**, 4195−4198.

Önal, M., Kahraman, S., and Sarıkaya, Y. (2007) Differentiation of α-cristobalite from opals in bentonites from Turkey. *Applied Clay Science*, **35**, 25−30.

Palaniandy, S. and Azizli, K.A.M. (2009) Mechanochemical effects on talc during fine grinding process in a jet mill. *International Journal of Mineral Processing*, **92**, 22−33.

Paterson, E. and Swaffield, R. (1987) Thermal analysis. Pp. 99−132 in: *A Handbook of Determinative Methods in Clay Mineralogy* (M.J. Wilson, editor). Chapman & Hall, London.

Prasad, B.K., Rathod, S., Modi, O.P., and Yadav, M.S. (2010) Influence of talc concentration in oil lubricant on the wear response of a bronze journal bearing. *Wear*, **269**, 498−505.

Ptáček, P., Lang, K., Šoukal, F., Opravil, T., Bartoníčková, E., and Tvrdík, L. (2014) Preparation and properties of enstatite ceramic foam from talc. *Journal of the European Ceramic Society*, **34**, 515−522.

Qin, H.L., Zhang, S.M., Zhao, C.G., and Yang, M.S. (2005) Zero-order kinetics of the thermal degradation of polypropylene/clay nanocomposites. *Journal of Polymer Science Part B: Polymer Physics*, **43**, 3713−3719.

Şahin, Ö., Özdemir, M., Aslanolu, M., and Beker, Ü.G. (2001) Calcination kinetics of ammonium pentaborate using the Coats-Redfern and genetic algorithm method by thermal analysis. *Industrial and Engineering Chemistry Research*, **40**, 1465−1470.

Sarıkaya, Y., Önal, M., Baran, B., and Alemdaroğlu, T. (2000) The effect of thermal treatment on some of the physicochemical properties of a bentonite. *Clays and Clay Minerals*, **48**, 557−562.

Schumann, D., Hartman, H., Eberl, D.D., Sears, S.K., Hesse, R., and Vali, H. (2013) The influence of oxalate-promoted growth of saponite and talc crystals on rectorite: testing the intercalation-synthesis hypothesis of 2:1 layer silicates. *Clays and Clay Minerals*, **61**, 342−360.

Şener, S. and Özyılmaz, A. (2010) Adsorption of naphthalene onto sonicated talc from aqueous solutions. *Ultrasonics Sonochemistry*, **17**, 932−938.

Smykatz-Kloss, W. (1974) *Differential Thermal Analysis, Application and Results in Mineralogy*. Springer, Berlin.

Tang, W.J., Liu, Y.W., Zhang, H., and Wang, C.X. (2003) New approximate formula for Arrhenius temperature integral. *Thermochimica Acta*, **408**, 39−43.

Terada, K. and Yonemochi, E. (2004) Physicochemical properties and surface free energy of ground talc. *Solid State Ionics*, **172**, 459−462.

Wang, D.J. and Karato, S.-i. (2013) Electrical conductivity of talc aggregates at 0.5 GPa: influence of dehydration. *Physics and Chemistry of Minerals*, **40**, 11−17.

Ward, J.R. (1975) Kinetics of talc dehydroxylation. *Thermochimica Acta*, **13**, 7−14.

Wesolowski, M. (1984) Thermal decomposition of talc: a review. *Thermochimica Acta*, **78**, 395−421.

Xu, X.F., Ding, Y.F., Wang, F., Wen, B., Zhang, J.H., Zhang, S.M., and Yang, M.S. (2010) Effects of silane grafting on the morphology and thermal stability of poly(ethylene terephthalate)/clay nanocomposites. *Polymer Composites*, **31**, 825−834.

Yang, H.M., Du, C.F., Hu, Y.H., Jin, S.M., Yang, W.G., Tang, A.D., and Avvakumov, E.G. (2006) Preparation of porous material from talc by mechanochemical treatment and subsequent leaching. *Applied Clay Science*, **31**, 290−297.

Yu, Y., Xue, G., Gu, C., Lou, J., and Li, S. (2013) Preparation of chitosan modified talc and its application in high filler content paper. *Journal of Applied Polymer Science*, **129**, 2692−2698.

Zulumyan, N.H., Papakhchyan, L.R., Isahakyan, A.R., Beglaryan, H.A., and Aloyan, S.G. (2012) The influence of mechanical treatment on the silicate network of talc. *Russian Journal of Physical Chemistry A*, **86**, 1008−1013.